Fabrication of Whitely Luminescent Silicon-Rich Nitride Films by Atmospheric Pressure Chemical Vapor Deposition

2008 Jpn. J. Appl. Phys. 47 4696

(http://iopscience.iop.org/1347-4065/47/6R/4696)

Japanese Journal of Applied Physics
Vol. 47, No. 6, 2008, pp. 4696–4699

Fabrication of Whitely Luminescent Silicon-Rich Nitride Films by Atmospheric Pressure Chemical Vapor Deposition

Chia-Hung LIN, Wu-Yih UEN*, Yen-Chin HUANG, Zhen-Yu LI[2], Sen-Mao LIAO, Tsun-Neng YANG[1], Shan-Ming LAN[1], and Yu-Hsiang HUANG[1]

Department of Electronic Engineering, College of Electrical Engineering and Computer Science, Chung Yuan Christian University, Chungli 32023, Taiwan
[1]*Institute of Nuclear Energy Research, P.O. Box 3-11, Lungtan 32500, Taiwan*
[2]*Department of Photonics and Institute of Electro-Optical Engineering, National Chiao Tung University, 1001 TA Hsueh Road, Hsinchu 30010, Taiwan*

(Received October 21, 2007; accepted February 4, 2008; published online June 13, 2008)

Silicon-rich nitride (SRN) films that can exhibit an intense white-light emission were fabricated by atmospheric pressure chemical vapor deposition. SRN films were deposited on Si substrates using gaseous SiH_2Cl_2 (DCS) and NH_3 as the source materials for Si and N, respectively. The deposition temperature was kept at 850 °C, and H_2 was used as the carrier gas with its flow rate modulated to maintain chamber pressure at 1 atm during the deposition. The optical properties of films obtained at various deposition times from 15 to 60 min were examined by photoluminescence (PL) measurement. An intense luminescence band (1.5–3.5 eV) was observed by the naked eye for all as-deposited samples. Besides, time-resolved PL exhibited a short radiative lifetime of about 1 ns for SRN films. Moreover, high resolution plan-view transmission electron microscopy demonstrated the existence of Si dots in SRN films with the dot sizes ranging from 2 to 6 nm and a dot density of about $4 \times 10^{12}/cm^2$. On the basis of the results obtained, we considered that the related luminescence mechanism for SRN films is connected to crystalline Si dots produced therein. [DOI: 10.1143/JJAP.47.4696]

KEYWORDS: SiN_x films, AP-HCVD, Si-QDs, HRTEM

1. Introduction

In recent years, Si-based light-emitting diodes (LEDs) have become very popular owing to their low cost of fabrication and easy integration with conventional IC technology compared with the present high-efficiency III–Vs-based LEDs. This naturally makes Si-based light-emitting materials some of the best for realizing optoelectronic integrated circuits (OEICs). The discovery of bright photoluminescence (PL) from electrochemically etched porous silicon (PSi) has led to much research on fabricating efficient Si-based LEDs.[1–4] However, the application of PSi has been limited by its unstable optical properties and physical fragility. Accordingly, other approaches to fabricating Si-based LEDs on silicon oxide (SiO_x) have gradually been developed, including the use of native SiO_x (NSO)[5–8] and Si-rich oxide (SRO),[9,10] doping or ion-implanting SiO_2 with various atoms, such as Si, Ge, Er^{3+}, and others,[11–13] inserting multiple quantum wells into a SiO_x film,[14] and growing Si/SiO_2 superlattices.[15] However, for LEDs fabricated from a SiO_x material, the applied working voltage is too high, and will be an issue for practical use.

Besides the materials mentioned above, silicon nitride (SiN_x) is also an alternative for Si-based LEDs. In particular, the potential barrier at a Si/Si_3N_4 interface is much lower than that at a Si/SiO_2 interface.[16] Therefore, for Si/SiN_x, conditions for carrier injection can be improved, so SiN_x has greater potential for fabricating white-light LED.[17]

In using a SiN_x material for white-light LEDs, basically a silicon-rich nitride (SRN) film with crystalline or amorphous Si quantum dots (QDs) embedded therein must be formed. So far, almost all these types of film have been fabricated by plasma-enhanced chemical vapor deposition (PECVD).[17–23] The main advantage of the PECVD method is its relatively low deposition temperatures (usually $\leq$400 °C). Compared with PECVD, atmospheric pressure CVD (APCVD) is another conventional deposition method for SiN_x films but can be a simpler fabrication process and cost-competitive for device applications of the SRN structure. Additionally, higher deposition temperatures in APCVD can be expected for achieving better material quality, such as lower pinhole density and better adhesion to the substrate. Nevertheless, the use of APCVD for fabricating whitely luminescent films has seldom been studied and relevant works are scarce.[24] Hence, in this paper, we present the results of our investigation on SRN films fabricated by APCVD. In particular, to our knowledge, this is the first time to recognize that APCVD can be used to fabricate SRN films with crystalline Si QDs embedded therein.

2. Experiment

The samples were prepared using a home-made one-flow APCVD system with a vertical chamber. The substrates used were 2-in. (111)-oriented, 1–2 Ω·cm p-type Si wafers. Before loading, the substrate was cleaned by boiling it in $H_2SO_4 : H_2O_2 = 3 : 1$ for 15 min and then dipped in HF solution ($HF : H_2O = 1 : 10$) for 15 s to obtain a stable hydrogen-passivated surface. Dichlorosilane (SiH_2Cl_2, DCS) and ammonia (NH_3) were used as the source materials for Si and N, respectively, and H_2 was the carrier gas. After loading, the substrate was initially heated to 1100 °C in H_2 ambient for 7 min, to remove the passivated layer on the surface. Then, SRN films were grown at a constant temperature of 850 °C and at a constant flow ratio of $[NH_3]/[DCS] = 1.2$ in an H_2 environment. The film deposition time was varied from 15 to 60 min.

The optical properties were examined by room-temperature photoluminescence (PL) measurement. PL spectra were excited with the 325 nm line of a He–Cd laser at excitation power densities of 0.1–0.25 kW/cm^2. The luminescence was dispersed by a 1 m monochromator and detected using a water-cooled GaAs photomultiplier. More-

*E-mail address: uenwuyih@ms37.hinet.net; mfamizuki@hotmail.com

over, radiative lifetime was determined from time-resolved photoluminescence (TRPL) measurement at room temperature. In this case, the signal was excited by a GaN semiconductor laser ($\lambda = 396$ nm) with a pulse width of about 0.15 ns and a power density of 0.2 W/cm^2. The thickness of SRN films was determined by scanning electron microscopy (SEM). The microstructure of the films was studied by plan-view high resolution transmission electron microscopy (HRTEM) using a Philips Tecnai F20 microscope operated at 200 keV. Specimens used for HRTEM were first chemically etched, then mechanically polished to <5 μm and finally ion-milled to achieve electron transparency.

3. Results and Discussion

Figure 1 shows the room-temperature PL spectrum of a typical SRN film deposited for 40 min (referred to below as sample SRN-A). As can be observed, a strong white luminescence band covers a range from 1.5 to 3 eV with three subpeaks at 2.08, 2.45, and 2.81 eV, individually. Two intervals among these peaks are 360 and 370 meV. Considering these large energy deviations, it is plausible that the aforementioned subpeaks did not result from Si QDs of different sizes nor the transitions between different energy levels in the same Si QD. The origin of these subpeaks will be analyzed in detail after Fig. 4 is presented. Now, to the spectrum shown in Fig. 1 a Gaussian distribution is fitted over the 1.5–3.5 eV range with the peak at 2.5 eV. Obviously, the luminescence peak energy is blue-shifted

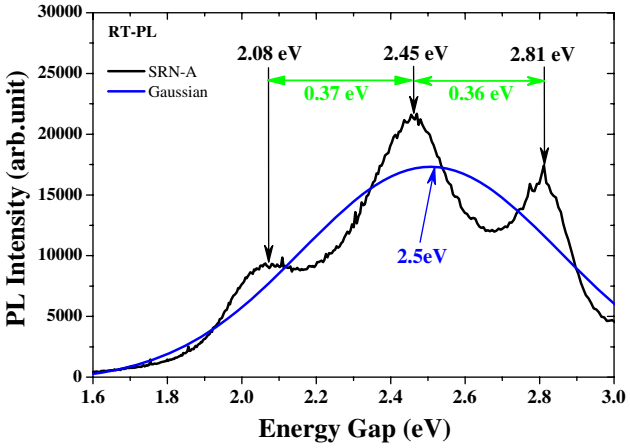

Fig. 1. (Color online) Room-temperature PL spectrum of sample SRN-A and Gaussian fitting to it.

from that of crystalline Si bulk (1.12 eV) by 1.38 eV. This result is considered to be related to the quantum confinement effect of Si QDs embedded in the matrix of amorphous SiN_x with a band-gap energy of approximately 5 eV,[25] as examined from both theoretical and experimental points of view described below.

As was reported, the Gaussian distribution of PL spectra from Si QDs demonstrates theoretically an ensemble of Si QDs of various sizes.[26] Otherwise, the effective band-gap energy of a Si QD modeled by a block with three unequal sizes, d_1, d_2, and d_3 can be given by[27]

$$E_{\mathrm{gap}} = E_{\mathrm{gap},0} + \frac{\pi^2\hbar^2}{2}\left(\frac{m_{\mathrm{l}}^{-1} + m_{\mathrm{h}}^{-1}}{d_1^2} + \frac{m_{\mathrm{t}}^{-1} + m_{\mathrm{h}}^{\perp -1}}{d_2^2} + \frac{m_{\mathrm{t}}^{-1} + m_{\mathrm{h}}^{\perp -1}}{d_3^2}\right), \quad (1)$$

where $E_{\mathrm{gap},0}$ is the indirect band gap of Si bulk at 300 K. As can be noted from the subsequent HRTEM image displaying Si QDs, it is reasonable to assume a spherical QD with an equivalent three-dimensional (3D) size $d = d_1 = d_2 = d_3$ and then eq. (1) can be simplified to

$$E_{\mathrm{gap}} = E_{\mathrm{gap},0} + \frac{C}{d^2}, \quad (2)$$

where C is the confinement parameter.[18,20,21]

The curves shown in Fig. 2 show the relationship between the effective band-gap energy and the size of a spherical QD for both crystalline and amorphous Si QDs. The curve in solid line is plotted for the former using eq. (2) with $E_{\mathrm{gap},0} = 1.12$ eV and $C \approx 8.845$ determined using the bulk parameters of Si given in ref. 27. Otherwise, the curve in dash line at the bottom is the same plot for the latter, as reported in refs. 18, 20, 21. Furthermore, for comparison, the plot in dot-dash line at the top is a copy of the curve fitting to the relationship between PL peak energy and the flow rate of $[SiH_4]/[N_2]$ for crystalline Si QDs examined in ref. 20. In the same reference the fitting parameters of $E_{\mathrm{gap},0}$ and C are resolved to be about 1.16 eV and 11.8, respectively. Using these curves and the parameters obtained from the Gaussian fitting to the PL spectrum, one can analyze the size distribution of Si QDs. The range (1.5–3.5 eV) and peak position (2.5 eV) of the Gaussian fitting curve shown in Fig. 1 are indicated in Fig. 2 by two open

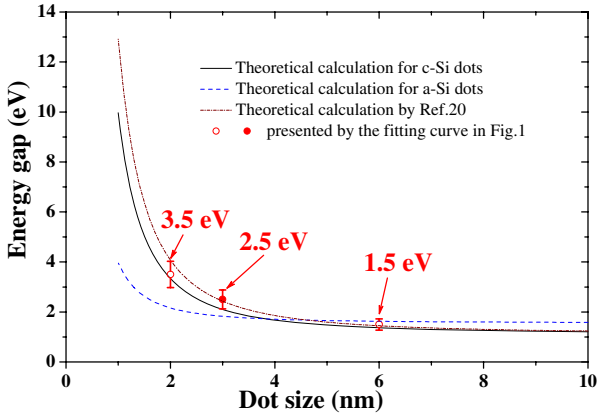

Fig. 2. (Color online) Relationship between effective band-gap energy and size of Si QD.

circles and one closed circle, respectively, with their measurement errors indicated. It is found that the luminescence energies of Si QDs in sample SRN-A can be well described by eq. (2) for the case of crystalline Si QD, from which information on a size distribution range of 2–6 nm for the crystalline Si QDs and that on the largest number of dots with a size of 3 nm were extracted.

On the other hand, for a direct observation of nanostructures, Fig. 3 shows a plan-view HRTEM image of

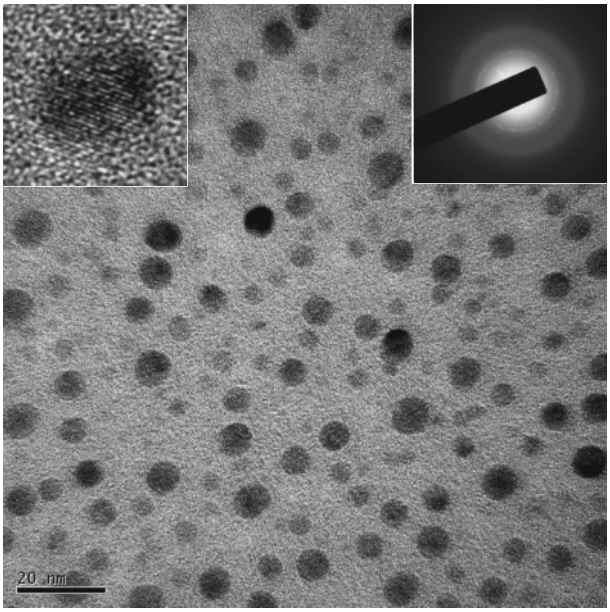

Fig. 3. Plan-view HRTEM image of sample SRN-A. The top left insert shows a magnified view of a crystalline Si QD and the top right inset shows the transmission electron diffraction pattern of the SRN film.

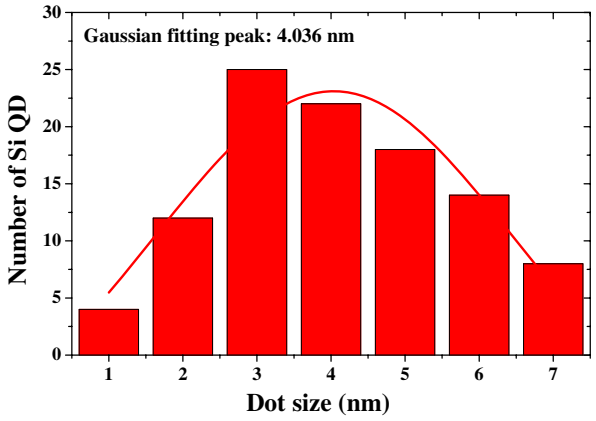

Fig. 4. (Color online) Number of Si QDs plotted as a function of dot size.

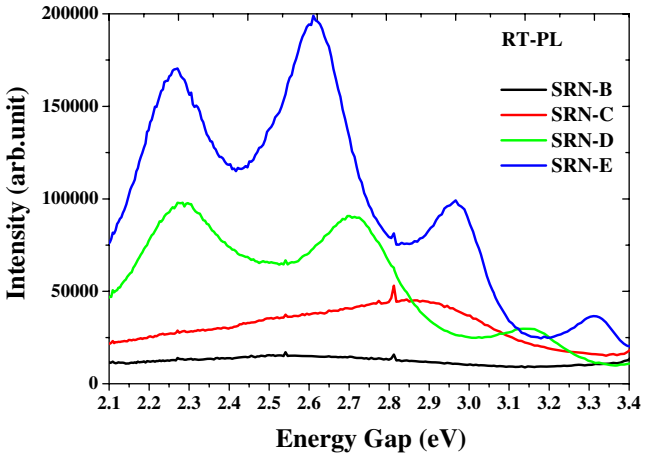

Fig. 5. (Color online) Room-temperature PL spectra of samples SRN-B, SRN-C, SRN-D, and SRN-E.

sample SRN-A showing a wide uniform distribution of dark nanoparticles. The top left inset of the figure shows a magnified image of a dark nanoparticle, whereas the top right inset shows the transmission electron diffraction (TED) pattern of the SRN film. Evidently, the top left inset shows that the dark nanoparticles in the SRN matrix demonstrate crystalline Si QDs, which are embedded in the amorphous SRN film. This condition is further confirmed by the TED pattern where well-defined spots in multiple directions are visible in a hollow background, showing that monocrystalline Si QDs in various orientations are generated in the SRN film. Several HRTEM images with scanning areas ranging from 50×50 to $100 \times 100\,\mathrm{nm}^2$ according to different magnifications were used to evaluate the average distribution of Si QDs in the SRN film. Figure 4 shows the number distribution of Si QDs as a function of dot size. As can be observed, the Si QDs embedded in the SRN film were also found to follow the Gaussian distribution having dot sizes ranging from 1 to 7 nm. The density of Si QDs was determined to be about $4 \times 10^{12}/\mathrm{cm}^2$. It therefore can be said that the size distribution of Si QDs estimated theoretically from Fig. 2 coincides with that determined directly from HRTEM images, as described above.

As demonstrated in Fig. 1, the white luminescence band shows three subpeaks at 2.08, 2.45, and 2.81 eV. It was indicated previously that the multiple interference phenomenon in PL spectra can be affected by film thickness.[28] In the present case, these peaks were also considered to be caused by multiple interference effects in the SRN film. In order to confirm this, we kept the flow ratio of $[NH_3]/[DCS]$ and growth temperature constant at 1.2 and 850 °C, respectively, but changed the growth time as 15, 30, 45, and 60 min to attain SRN films of different thicknesses, referred to below as samples SRN-B, SRN-C, SRN-D, and SRN-E, respectively. SEM images of these samples helped determine their film thicknesses to be 21.3, 269.4, 620.3, and 789.1 nm, respectively. Moreover, Fig. 5 shows the room-temperature PL spectra obtained from these films. As is shown, the appearance of subpeaks in the PL band becomes more evident as the SRN film becomes thicker. Nearly only one wide PL band is observed when the SRN film is thinner than 300 nm, whereas this wide band develops into two or three subbands with spacings of 360 and 355 meV when the SRN film is thicker than 600 nm.

Figure 6 shows the room-temperature TRPL spectra of the samples SRN-B, SRN-C, SRN-D, and SRN-E monitored at an energy of 2.48 eV (500 nm). Notably, normalized intensity is plotted on a semilogarithmic scale versus time on a linear scale. Evidently, the decay is not single exponential. The transient can be well fitted by a stretched exponential,[29–31] which is given by the following equation.

$$I(t) = I_0 \exp\left[-\left(\frac{t}{\tau}\right)^{\beta}\right], \tag{3}$$

where $I(t)$ is the PL intensity at time t and $I_0 \equiv I(0)$. The decay time constant τ is the average lifetime, and the dispersion factor β varies between zero and unity, providing information on the recombination mechanism. Table I shows the average lifetime and dispersion factor extracted from the fitting of eq. (3) to the PL decay spectra shown in Fig. 6. It can be observed that lifetime increases from 0.56 to

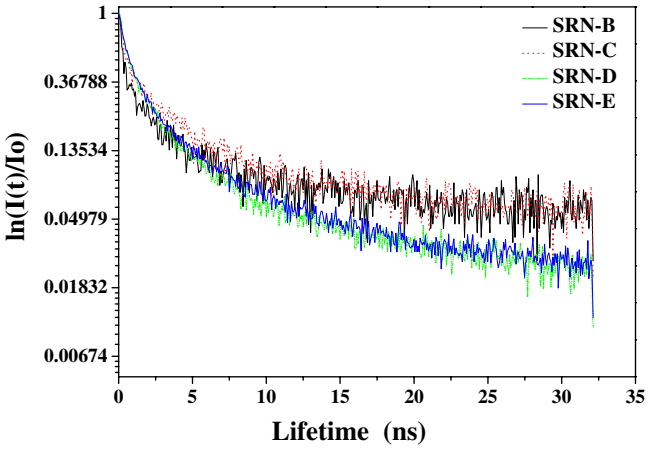

Fig. 6. (Color online) Room-temperature TRPL spectra of samples SRN-B, SRN-C, SRN-D, and SRN-E monitored at an energy of 2.48 eV. Curves are normalized and plotted on a semilog vs linear scale.

Table I. Average lifetimes and dispersion factors extracted from fitting of eq. (3) to data shown in Fig. 6.

Sample	Thickness (Å)	τ (ns)	β
SRN-B	213	0.56	0.5
SRN-C	2694	0.98	0.5
SRN-D	6203	1.07	0.6
SRN-E	7891	1.12	0.6

1.12 ns with increasing film thickness, whereas β ranges between 0.5 and 0.6. In particular, the lifetime approaches 1 ns when the film thickness is higher than 2600 Å. The magnitude scale of the average lifetime and the stretched exponential decay behavior of PL intensity might also suggest the luminescence mechanism of the SRN film grown in the present study to be the quantum confinement effect.[32] Additionally, it is worth noting that the lifetime seems to be influenced by film thickness. This is possibly because different sizes of Si QDs are formed when the SRN film is grown to different thicknesses. Nevertheless, to elucidate this in further detail, further study in this area must be conducted.

4. Conclusions

Silicon-rich-nitride films with Si QDs embedded inside were successfully deposited on the Si substrate by APCVD. PL measurements indicated an intense white luminescence band (1.5–3.5 eV) that can be observed by the naked eye and HRTEM observations demonstrated the existence of Si QDs in the grown films with dot sizes ranging from 2 to 6 nm and a dot density of about $4 \times 10^{12}/\mathrm{cm}^2$. The white PL band was considered to be basically associated with the quantum confinement effect of Si QDs; however, the PL spectral feature was also influenced by the multiple interference effects of the SRN film as the film was grown to over 600 nm. Additionally, a short radiative lifetime of about 1 ns was exhibited by time-resolved PL. The establishment of the experimental procedure for obtaining such a strong white light emission may lead to a significant progress towards the application of APCVD-grown SRN films to light-emission Si-based devices.

Acknowledgements

The authors would like to thank the National Science Council of Taiwan, for financially supporting this research under Contract NSC 95-2623-7-033-002-NU. The authors Uen and Lin are also grateful to the Institute of Nuclear Energy Research (INER) for technical assistance.

1) N. Koshida and H. Koyama: Appl. Phys. Lett. **60** (1992) 347.
2) B. Gelloz, T. Nakagawa, and N. Koshida: Appl. Phys. Lett. **73** (1998) 2021.
3) J. Linnros and N. Lallic: Appl. Phys. Lett. **66** (1995) 3048.
4) S. Lazarouk, P. Jaguiro, S. Katsouba, G. Mashini, S. La Monica, G. Maiello, and A. Ferrari: Appl. Phys. Lett. **68** (1996) 1646.
5) G. G. Qin, Y. M. Huang, B. Q. Zong, L. Z. Zhang, and B. R. Zhang: Superlattices Microstruct. **16** (1994) 387.
6) G. F. Bai, Y. Q. Wang, Z. C. Ma, W. H. Zong, and G. G. Qin: J. Phys.: Condens. Matter **10** (1998) L717.
7) Y. Q. Wang, T. P. Zhao, J. Liu, and G. G. Qin: Appl. Phys. Lett. **74** (1999) 3815.
8) J. Yuan and D. Haneman: J. Appl. Phys. **86** (1999) 2358.
9) D. J. DiMaria, J. R. Kirtley, E. J. Pakulis, D. W. Dong, T. S. Kuan, F. L. Pesavento, T. N. Theis, J. A. Cutro, and S. D. Brorson: J. Appl. Phys. **56** (1984) 401.
10) G. G. Qin, A. P. Li, and Y. X. Zhang: Phys. Rev. B **54** (1996) R11122.
11) Y. Liu, T. P. Chen, Y. Q. Fu, M. S. Tse, J. H. Hsieh, P. F. Ho, and Y. C. Liu: J. Phys. D **36** (2003) L97.
12) X. M. Wu, M. J. Lu, and W. G. Yao: Surf. Coat. Technol. **161** (2002) 92.
13) D. Pacifci, A. Irrera, G. Franzó, M. Miritello, F. Iacona, and F. Priolo: Physica E **16** (2003) 331.
14) M. Zacharias, J. Bläsing, P. Veit, L. Tsybeskov, K. Hirschman, and P. M. Fauchet: Appl. Phys. Lett. **74** (1999) 2614.
15) M. Zacharias, J. Heitmann, R. Scholz, and U. Kahler: Appl. Phys. Lett. **80** (2002) 661.
16) V. A. Volodin, M. D. Efremov, V. A. Gritsenko, and S. A. Kochubei: Appl. Phys. Lett. **73** (1998) 1212.
17) N. M. Park, T. S. Kim, and S. J. Park: Appl. Phys. Lett. **78** (2001) 2575.
18) N. M. Park, C. J. Choi, T. Y. Seong, and S. J. Park: Phys. Rev. Lett. **86** (2000) 1355.
19) K. S. Cho, N. M. Park, T. Y. Kim, K. H. Kim, G. Y. Sung, and J. H. Shin: Appl. Phys. Lett. **86** (2005) 071909.
20) T. Y. Kim, N. M. Park, K. H. Kim, G. Y. Sung, Y. W. Ok, T. Y. Seong, and C. J. Choi: Appl. Phys. Lett. **85** (2004) 5355.
21) T. W. Kim, C. H. Cho, B. H. Kim, and S. J. Park: Appl. Phys. Lett. **88** (2006) 123102.
22) L. D. Nergo, J. H. Yi, L. C. Kimerling, S. Hamel, A. Williamson, and G. Galli: Appl. Phys. Lett. **88** (2006) 183103.
23) M. Wang, D. Li, Z. Yuan, D. Yang, and D. Que: Appl. Phys. Lett. **90** (2007) 131903.
24) V. V. Vasilev, I. P. Mikhailovskii, and K. K. Svitashev: Phys. Status Solidi A **95** (1986) K37.
25) S. M. Sze: *Physics of Semiconductor Devices* (Wiley, New York, 1981) 2nd ed., p. 852.
26) F. Iacona, G. Franzo, and C. Spinella: J. Appl. Phys. **87** (2000) 1295.
27) J. B. Khurgin, E. W. Forsythe, G. S. Tompa, and B. A. Khan: Appl. Phys. Lett. **69** (1996) 1241.
28) D. C. Marra, E. S. Aydil, S. J. Joo, E. Yoon, and V. I. Srdanov: Appl. Phys. Lett. **77** (2000) 3346.
29) K. Yamaguchi, K. Mizushima, and K. Sassa: Appl. Phys. Lett. **77** (2000) 3773.
30) Pavesi L: J. Appl. Phys. **80** (1996) 216.
31) A. Y. Kobitski, K. S. Zhuravlev, H. P. Wagner, and D. R. T. Zahn: Phys. Rev. B **63** (2001) 115423.
32) X. Chen, B. Henderson, and K. P. O'Donnell: Appl. Phys. Lett. **60** (1992) 2672.